LA-UR-14-22458
Approved for public release; distribution is unlimited.

Title: SMIS PBX-9502 Test Report

Author(s): Marr-Lyon, Mark
Sandoval, Thomas D.
Herrera, Dennis H.

Intended for: Test report for sponsor
Report

Issued: 2014-04-11

SMIS PBX-9502 Test Report

Mark J. Marr-Lyon, Thomas D. Sandoval, Dennis H. Herrera

April 2014

1 Abstract

Two impact experiments in the Specific Munitions Impact Scenario (SMIS) configuration [1–3] were performed on September 3 and 4, 2013 at Lower Slobbovia firing site. Targets of the high explosive PBX-9502 were impacted with 1/2-inch diameter low-carbon steel spheres fired from a 30-mm powder gun at velocities of approximately 2.5 km/s. In one experiment the target was cased in a steel cylinder with steel end plates, and in the second the target was cased in a plastic cylinder with a thin steel front cover plate and a thick steel rear plate. In neither experiment did the PBX-9502 detonate, though some material reacted in the impact.

2 Experimental setup

Figure 1 shows the location of the components of the setup. The muzzle of the 30-mm gun is located about 5 m away from the sabot stripper plate. This gives the sabot time to open up and start to move away from the projectile. The sabot stripper plate is a 2.5 cm thick steel plate with a hole in the center to allow the projectile to pass through, but block the pieces of the sabot. Approximately 1 m after the stripper plate are the trigger screens to measure the input velocity. Four trigger screens are used: two screens, MS1 and MS2, where the projectile completes a circuit (Whithner make screen PT#0606600600MKPTE[1]), and two screens, BS1 and BS2, where the projectile breaks a circuit (Whithner break screen PT#0606600600). BS1, MS2, and BS3 are located 0.6 cm, 91.4 cm, and 92.1 cm downrange from MS1, respectively. The trigger screen MS3 is attached to the front of the target using tape and is used to trigger the x-ray and high-speed video diagnostics. Due to the thickness of the mounting plates, MS3 is positioned 27 mm (1.1 in) in front of the target. Not shown in figure 1 is a remotely-operated barrier between the gun and the stripper plate, which is intended to keep the projectile from striking an energetic target in the event of an accidental firing of the gun. The timing signals from the trigger screens were recorded on Tektronix TDS5054 oscilloscopes.

A single 1 MeV X-Ray source was positioned to take a flash radiograph of the impact (figure 2). A Photron SA5 camera was used to record video of the impact at 7,500 frames per second.

Three PDV probes were positioned to measure the velocity of the back plate. These were primarily to be used in the event of an energetic reaction to the impact, where the plate velocity could be used to infer the strength of the reaction. A probe was aimed at the center of the back plate and two more probes were positioned 2.5 cm (1 in) above and below the center probe.

Three rails located 90 degrees apart and containing seven piezoelectric pins each separated by 1.3 cm (0.5 in) were installed to detect the arrival time of the pressure wave at the outer surface of the cylinder. Four additional pins were installed 90 degrees apart through the front retaining ring at an angle such that the face of the pin touched the front steel plate. These pins were intended to measure the location of the projectile impact on the plate. However, since these pins interfered with the main pin rails they needed to be rotated relative to the pin rails and their location is not well known. For this reason, and because the returned signals were quite weak, the front-plate pins were of limited utility.

[1]Whithner Screen Graphics, LLC, www.whithner.com

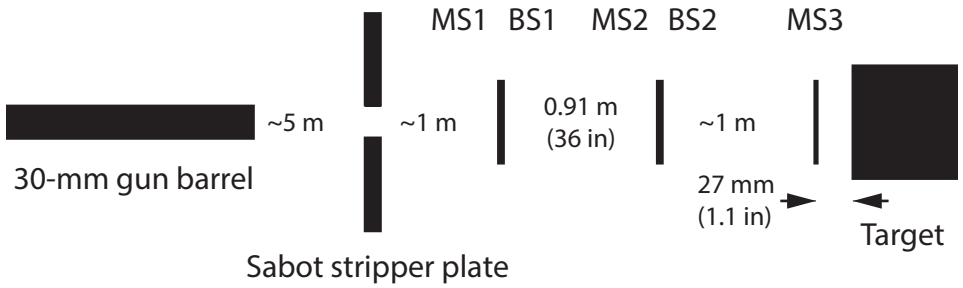

Figure 1: Relative locations of the gun, sabot stripper plate, velocity-measuring screens, and target.

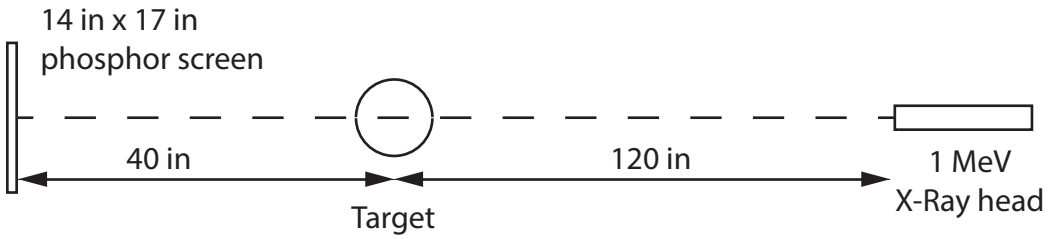

Figure 2: X-ray head location. The point of view is from the gun looking at the target.

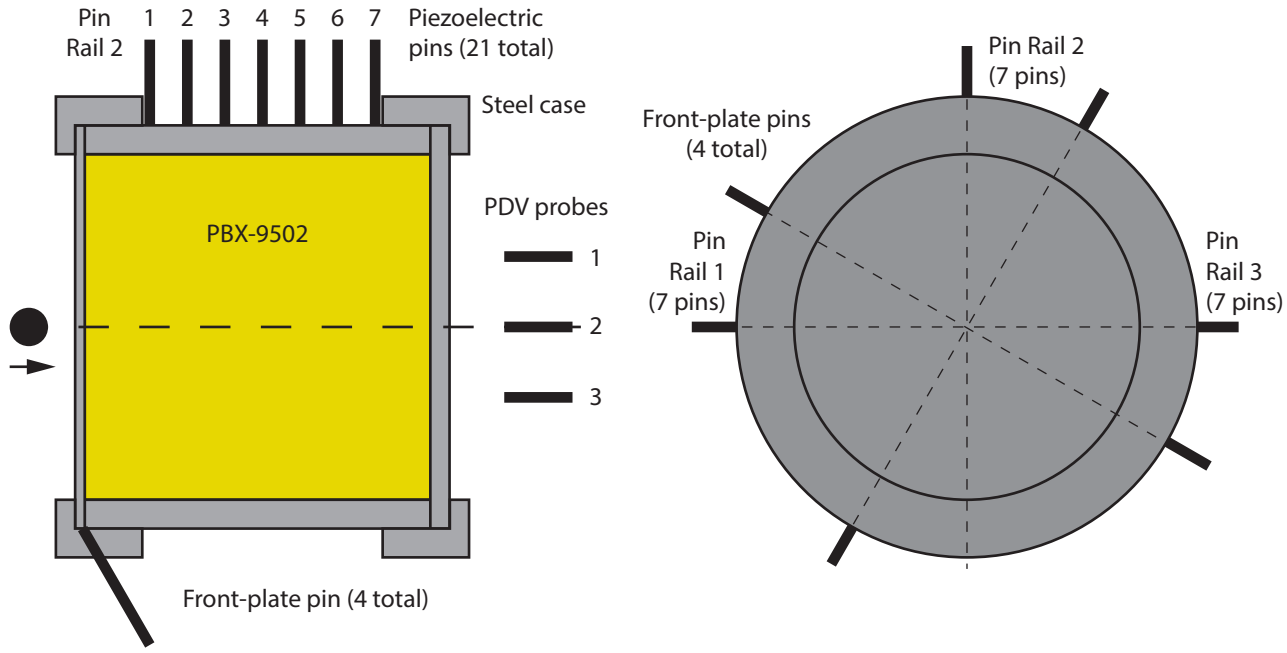

Figure 3: The target configuration for K12-21556. On the left is a cross-section view from the side, with the projectile striking the left surface. On the right is a front view showing the location of the pin rails and approximate location of the front-plate pins.

2.1 K12-21556

The target for shot K12-21556 (figures 3 and 4) was an 11.4 cm (4.5 in) diameter by 11.4 cm (4.5 in) long cylinder of PBX-9502 contained in a 1018 steel cylinder with a 9.3 mm (0.368 in) wall thickness. The cylinder has external threads on each end and 1018 steel retaining rings are used to hold 1018 steel plates over the end of the PBX-9502 cylinder. The plate on the impact side of the target was 3.2 mm (0.125 in) thick and the plate on the rear side of the cylinder was 6.4 mm (0.250 in) thick. During assembly, a thin layer of Sylgard 186 was spread on each end of the PBX-9502 cylinder.

The target was held between two 46 cm (18 in) square by 2.5 cm (1 in) thick polycarbonate plates. The pin rails were also attached to these plates. Pre-shot images of the target and mounting plates are shown in figure 4.

2.2 K12-21570

The target for shot K12-21570 (figures 5 and 6) was an 11.4 cm (4.5 in) diameter by 3.8 cm (1.5 in) long cylinder of PBX-9502 stacked on a 11.4 cm (4.5 in) diameter by 7.6 cm (3.0 in) long cylinder of 1018 steel and contained in a polycarbonate cylinder with a 9.3 mm (0.368 in) wall thickness. The PBX-9502 cylinder was rough-cut from a longer cylinder, and the rougher surface was placed next to the steel cylinder away from the impact side. The polycarbonate cylinder has external threads on each end and polycarbonate retaining rings are used to hold 1018 steel plates over the end of the PBX-9502 and steel cylinders. Windows were cut into the wall of the polycarbonate cylinder such that the piezoelectric pins were in contact with the inner cylinders. The plate on the impact side of the target was 3.2 mm (0.125 in) thick and the plate on the rear side of the cylinder was 6.4 mm (0.250 in) thick. During assembly, a thin layer of Sylgard 186 was spread on each end of the PBX-9502 cylinder.

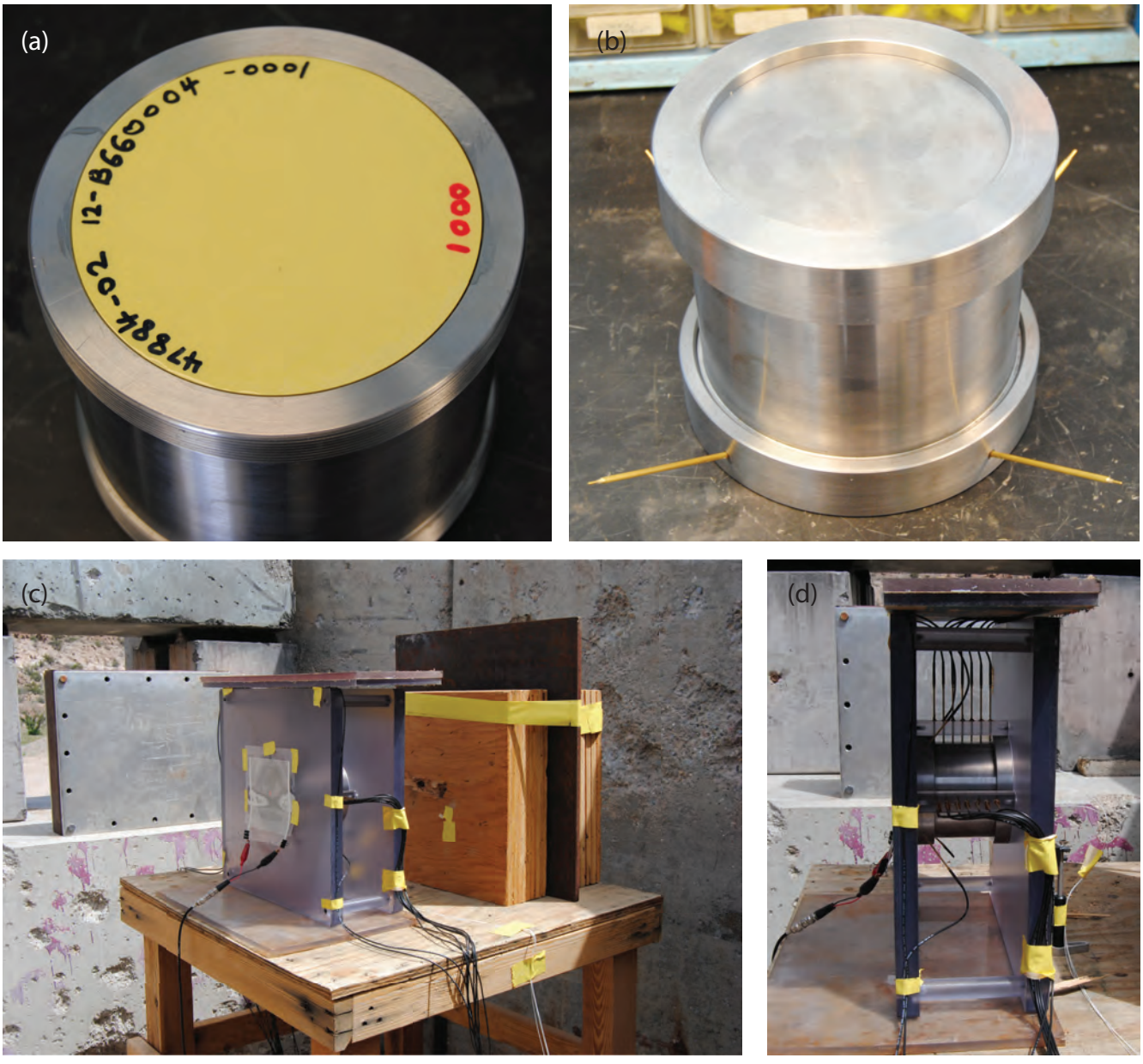

Figure 4: Pre-shot images for K12-21556. (a) The PBX-9502 cylinder in the steel cylinder. The threads used to attach the retaining rings are visible. (b) The back plate of the target. The four front-plate pins are mounted through the front retaining ring. (c) The target assembly in position. MS3 is covering the view of the front of the target. The x-ray cassette holder is in position to the left, and the projectile back stop is to the right of the target. (d) Side view of the target assembly showing pin rails. The PDV probe mounting hardware and fibers are visible to the left.

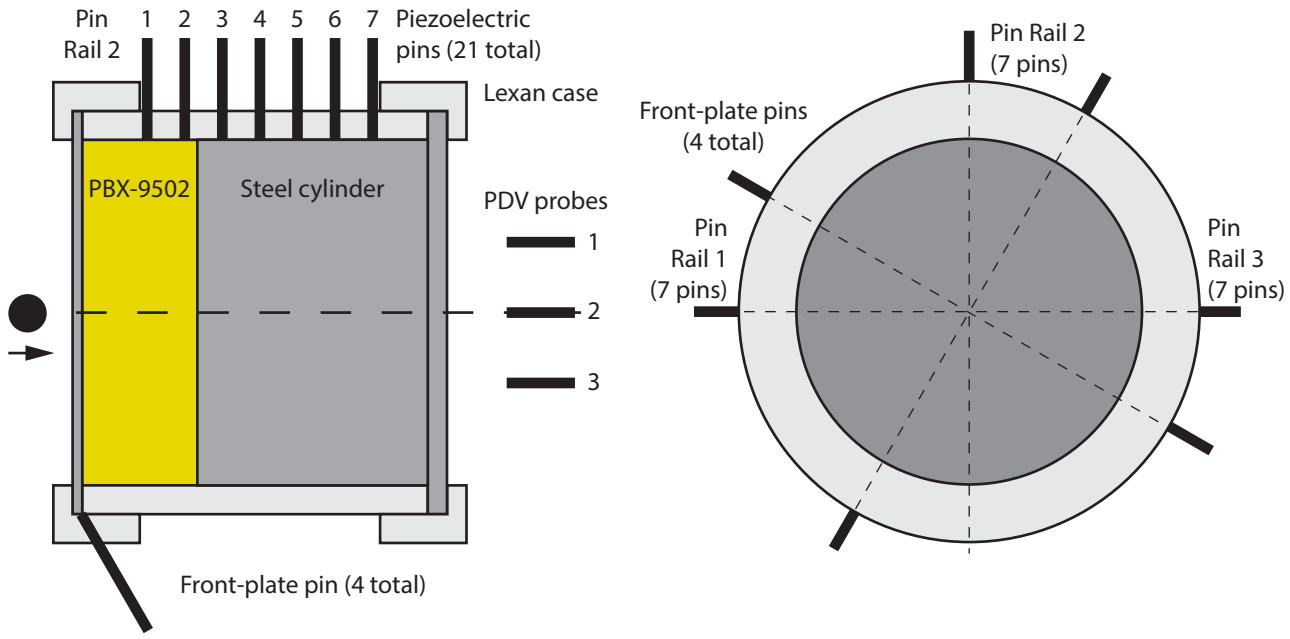

Figure 5: The target configuration for K12-21570. On the left is a cross-section view from the side, with the projectile striking the left surface. On the right is a front view showing the location of the pin rails and approximate location of the front-plate pins.

Figure 6: Pre-shot photographs of K12-21570. On the left is a side view of the target cylinder. On the right is a view of the target assembly, x-ray phosphor cassette, and two turning mirrors for the high-speed camera.

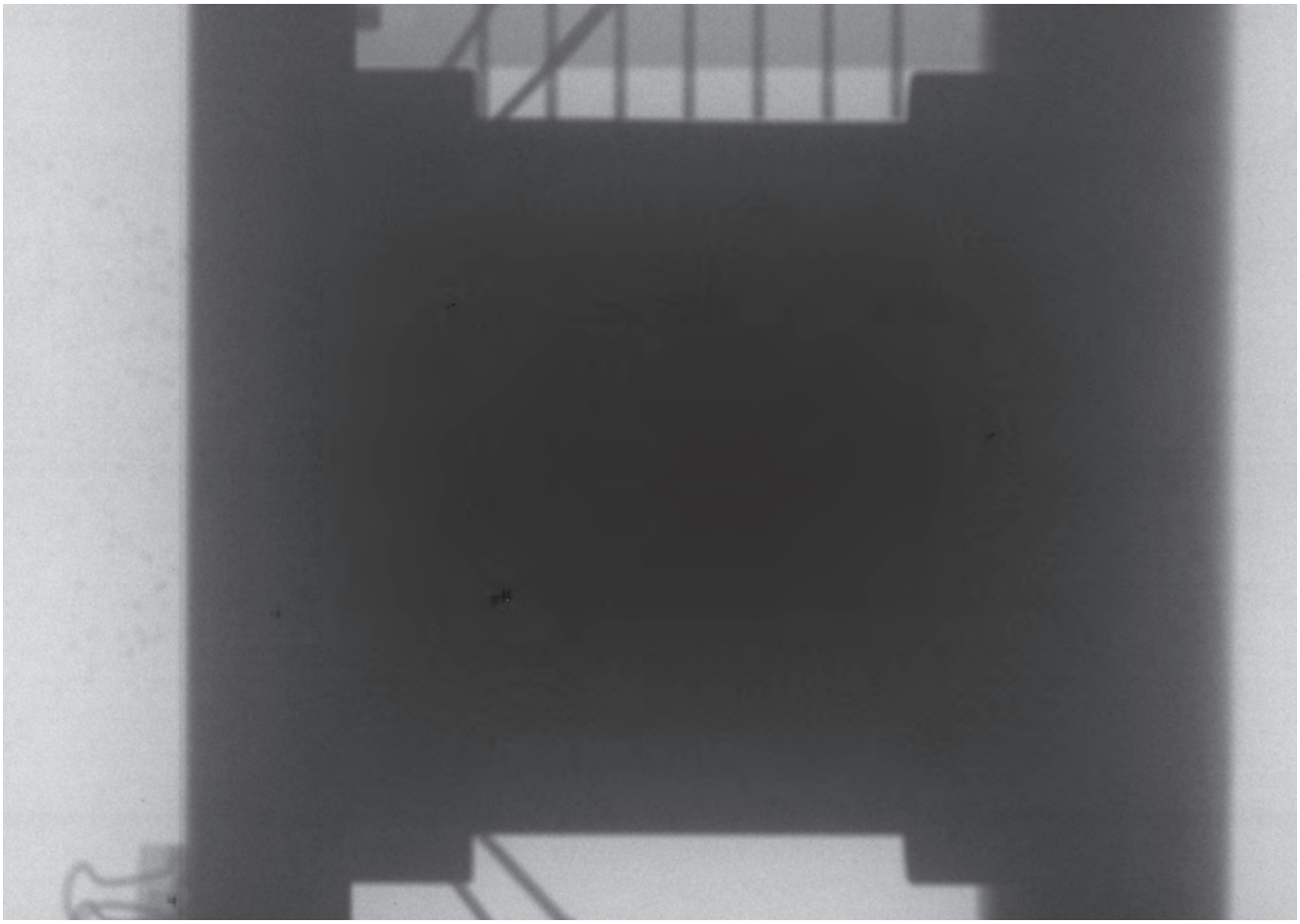

Figure 7: This radiograph of K12-21556 was taken 50 μs after the projectile triggered MS3.

3 Results

3.1 K12-21556

Only two of the four velocity measuring screens returned signals for this shot. From the two that did return signals, the impact velocity was 2.462 km/s. No estimate on the error in velocity can be made.

A single flash radiograph was taken 50 μs after MS3. This radiograph was intended to show the extent of a violent reaction should it occur. Since there was no reaction, there is little to be seen in the image. The 1 MeV x-rays did not sufficiently penetrate the target to resolve any damage inside the target, and all that is visible is the spray of steel fragments produced by the impact with the front plate on the left of the image.

Frames from the high-speed video of the impact are shown in figure 8. At $t = -0.133$ ms, the blurred projectile can be seen. At $t = 0$ ms, the projectile has triggered MS3. A bright flash is seen followed by about 8 ms of flames. The bright white spots on the right side of the frames at $t = 3.867$ ms and $t = 12.133$ ms are damage to the turning mirror closest to the target caused by fragments produced in the impact. For about 40 ms after the flames have extinguished, PBX-9502 can be observed pouring out of the impact hole until the view is obscured by propellant gases.

As the steel confinement cylinder remained intact, a significant amount of post-shot analysis

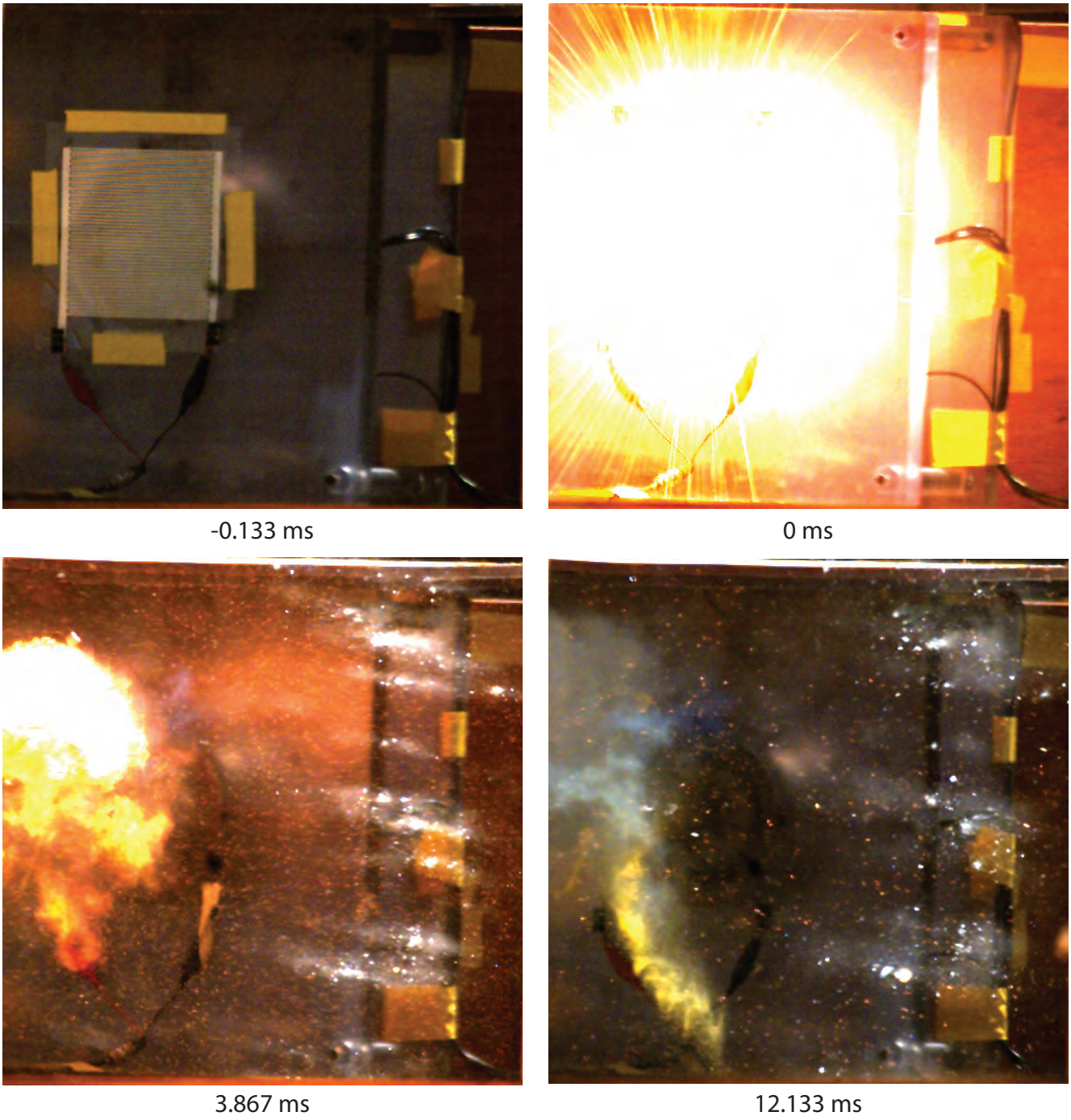

Figure 8: Frames from the high-speed video of K12-21556.

Figure 9: Post-shot photographs of K12-21556. The front plate has bulged considerably, and PBX-9502 fragments are visible through the entry hole. The cylinder wall has also bulged in the impact.

could be performed. Post-shot photographs are shown in figure 9. The cavity behind the entry hole was completely filled with PBX-9502 fragments and the front plate is significantly bulged. There was also some deformation to the cylindrical wall as well as the back plate. Apart from the entry hole, there are no other breaches to the steel confinement.

As with the radiograph, the PDV probes were intended to provide a measurement of the back plate velocity in the event of an energetic reaction. Figure 10 shows the measured velocities and positions of the back plate at the three probe locations. All the velocities are in the 50 to 60 m/s range, with displacements of 7 to 10 mm over the integration time.

Interpretation of the results from the piezoelectric pins is made more complicated by the fact that the path of the disturbance from the impact to the pin is not known. However, an effective velocity can be calculated by simply dividing the distance from the impact point by the time between impact and received signal. The distance between the impact location and the pin rails was measured by analysis of post-shot images and accounted for in the calculation shown in figure 11. While the effective velocity at the first pin location is similar for all three rails, rail 1 diverges after pin 1 and is consistently higher than the other two rails. Pin 7 did not return a signal for rails 2 or 3. The dents in the steel cylinder left by colliding with the pins are shown in figure 12 and confirm that pin 7 did not leave a dent for either rail 2 or 3. The dents are more defined for pins closer to the impact.

Three post-shot static radiographs (figure 13) were taken along orthogonal axes. The radiographs show the projectile penetrating about halfway into the PBX-9502. The projectile has broken into several pieces, with perhaps one large main fragment. Cracks in the PBX-9502 are also visible.

After the post-shot radiographs were taken, the pieces of PBX-9502 and ball fragments were removed through the entry hole (figure 14). Approximately 270 g of PBX-9502 was recovered, as well as many metal fragments. The pre-shot mass of the steel cylinder, flanges, end plates, and PBX-9502 was 8.63 kg, and the post-shot mass of the target assembly plus recovered material is 8.61 kg. This places an upper bound on the amount of PBX-9502 that reacted during the experiment of 20 g, or 0.9% of the initial charge mass. Some steel and PBX-9502 was not recovered after the experiment, so the amount of reacted PBX-9502 is certainly less than the full 20 g.

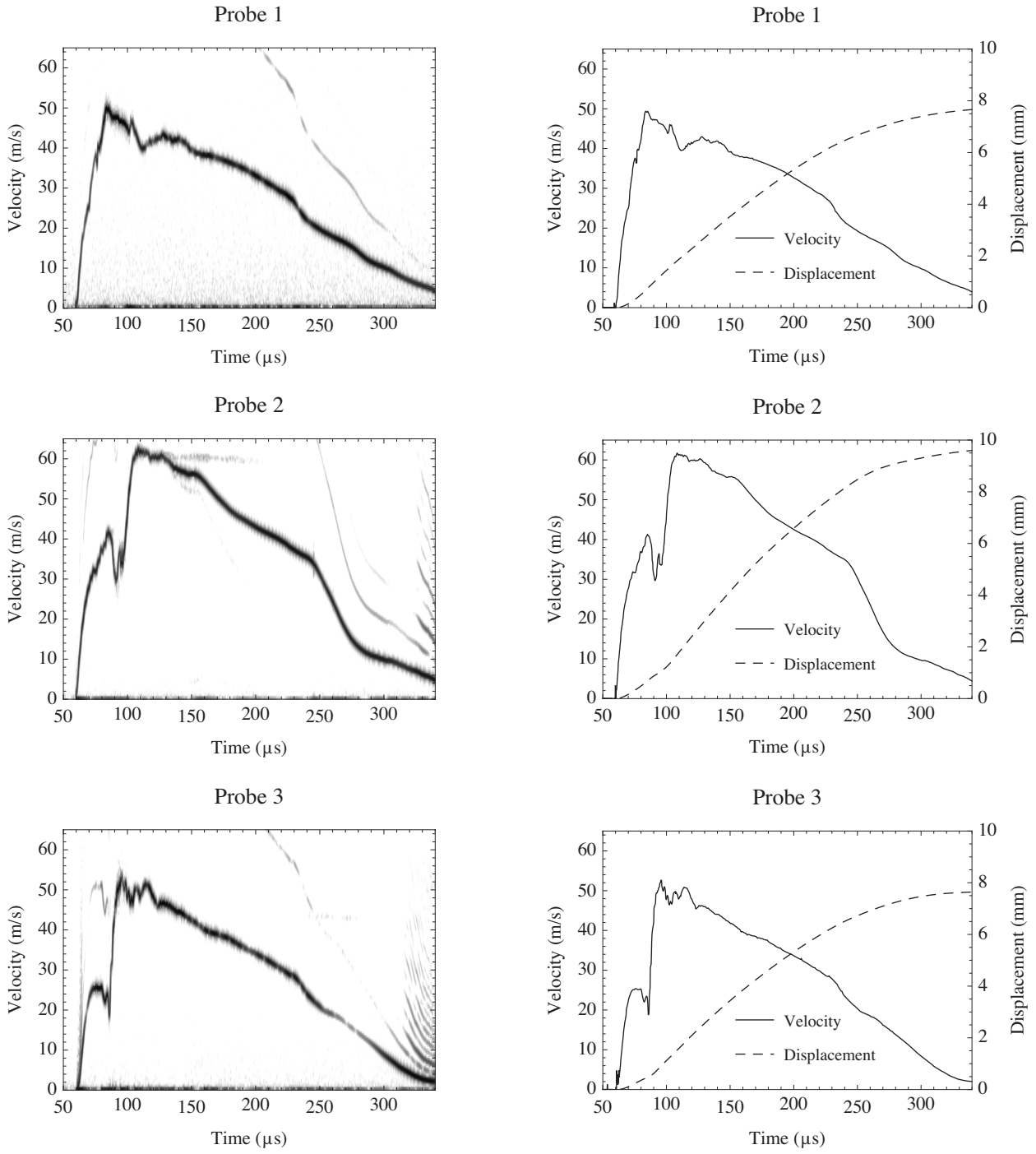

Figure 10: PDV data for K12-21556. The spectrograms are shown in the left column. Extracted velocities and integrated displacements are shown in the right column.

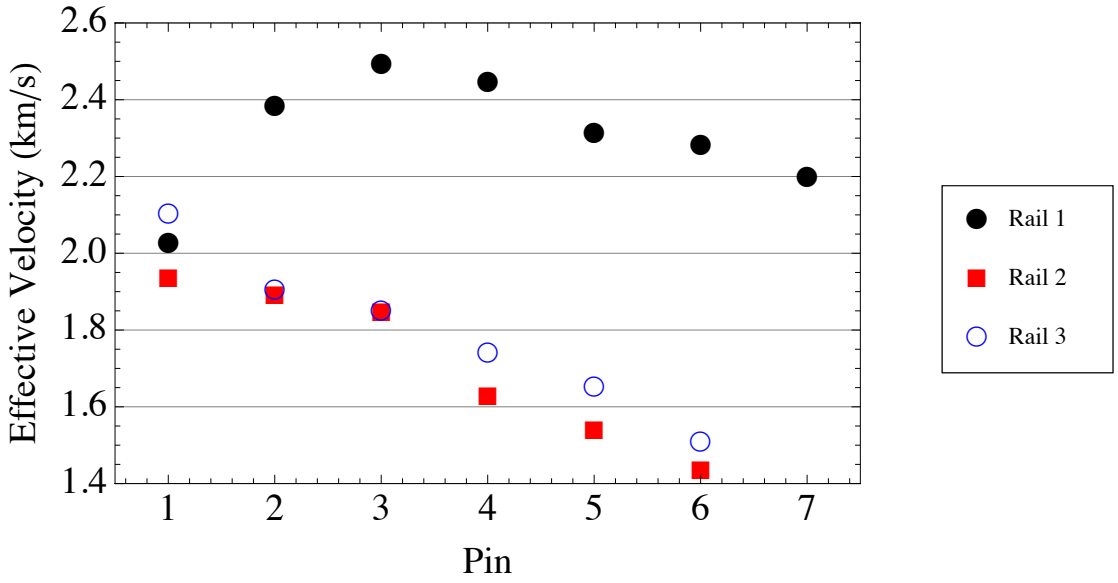

Figure 11: Effective velocity of the disturbance from the impact point to the pin location for shot K12-21556.

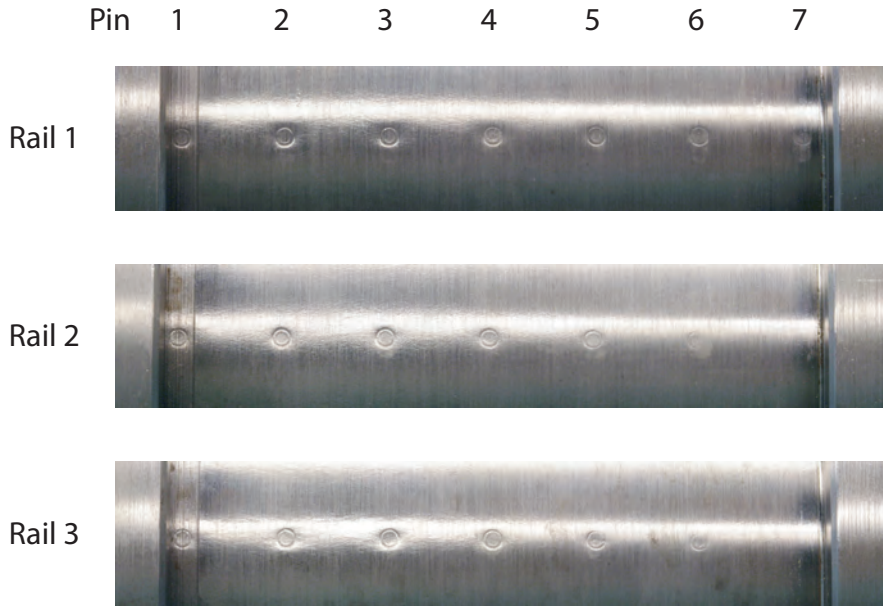

Figure 12: Dents resulting from the piezoelectric pins. Pin 7 on rails 2 and 3 did not leave a dent or return a signal.

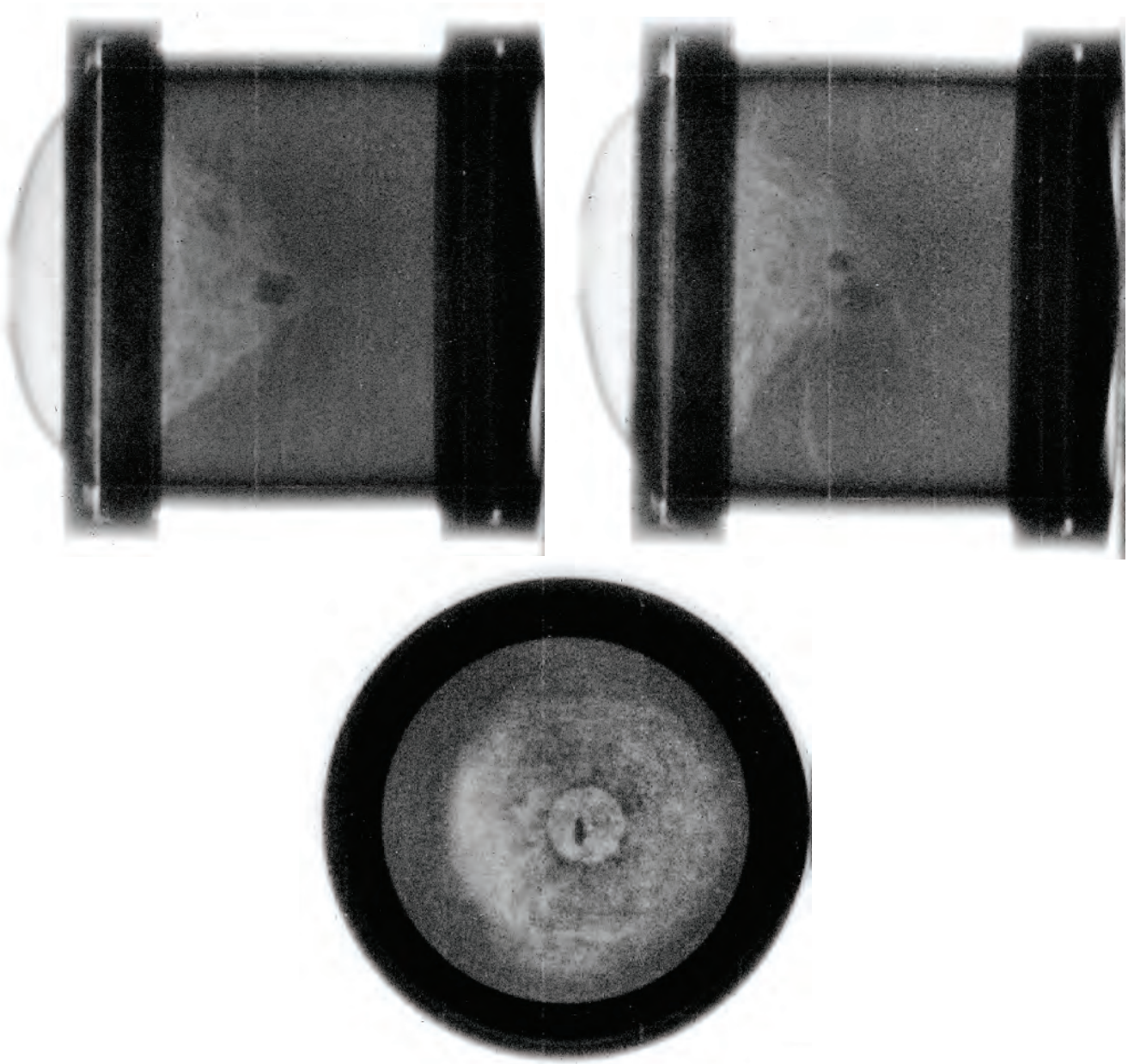

Figure 13: Post-shot radiographs of K12-21556 taken along three orthogonal axes. The horizontal and vertical lines are caused by tile boundaries in the detector.

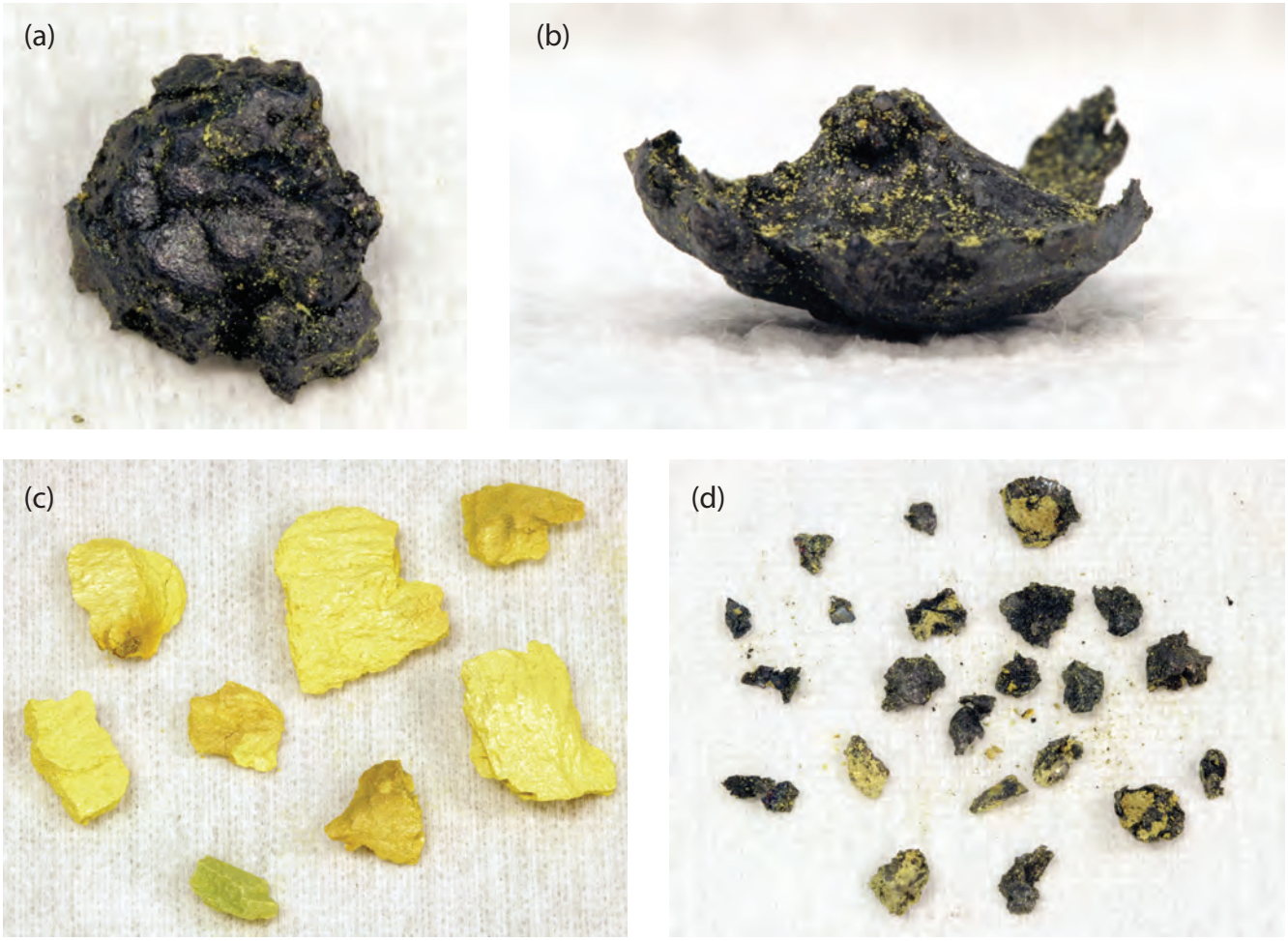

Figure 14: Recovered metal and HE fragments from the K12-21556 target. (a) Impact face of the largest projectile fragment, approximately 1 cm in diameter. (b) Profile of the largest projectile fragment showing the central protruberance on the back surface. (c) PBX-9502 fragments, some of which are still the same color as unimpacted PBX-9502, some of which have been scorched during the impact, and one of which has turned green. The largest piece is approximately 3 cm long. (d) Other metal fragments, all of which are smaller than (a).

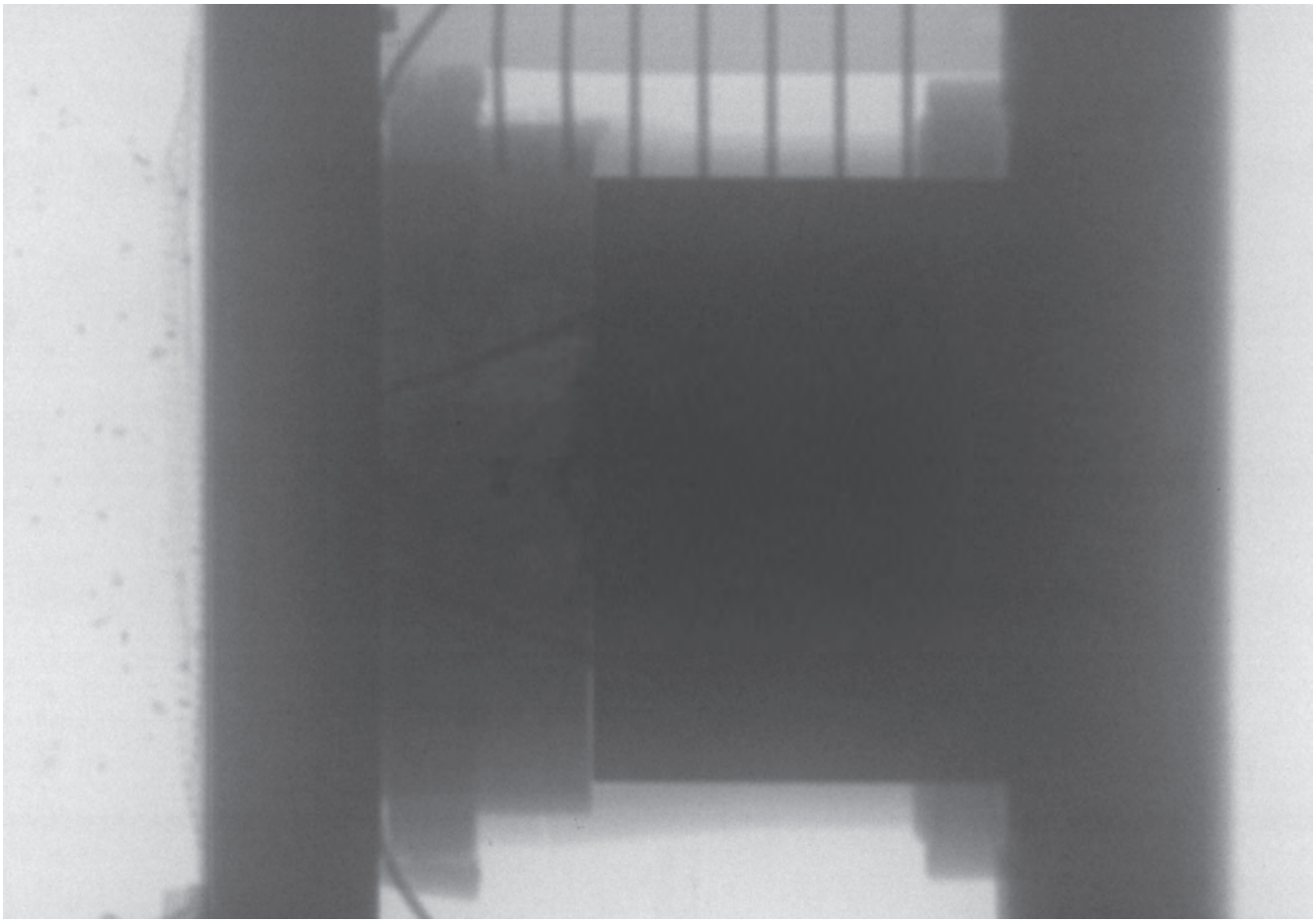

Figure 15: This radiograph of K12-21570 was taken 100 μs after the projectile triggered MS3.

3.2 K12-21570

Since K12-21570 was fired after K12-21556, it was expected that the PBX-9502 would not detonate, and the time between MS3 trigger and the radiograph (figure 15) was lengthened to 100 μs. Without the steel cylinder surrounding the explosive, some detail can be resolved. Some expansion of the PBX-9502 is seen, and a cavity inside the PBX-9502 is partially visible.

The measured velocity of the projectile prior to impact was 2.433 ± 0.002 km/s. Frames from the high-speed video of the impact are shown in figure 16. At $t = -0.133$ ms, the blurred projectile can be seen. At $t = 0$ ms, the projectile has triggered MS3. A bright flash is seen followed by about 5 ms of flames. The bright white spots on the right side of the frames at $t = 3.733$ ms and $t = 7.467$ ms are damage to the turning mirror closest to the target caused by fragments produced in the impact. Initially the impact is very similar to that in K12-21556. Immediately after the impact, the polycarbonate cylinder fails resulting in PBX-9502 being widely dispersed.

The steel cylinder and front plate as found after the shot are shown in figure 17. Only a small dent was produced by the projectile striking the steel cylinder. As the front plate was more deformed in the impact than in K12-21556, the location of the impact relative to the center of the plate could not be determined in the same manner. Because of this, the effective velocities in figure 18 were calculated assuming an impact in the exact center and rail-to-rail comparisons are not meaningful. The first two pins of each rail were initially in contact with the PBX-9502, and pins 3 through 7

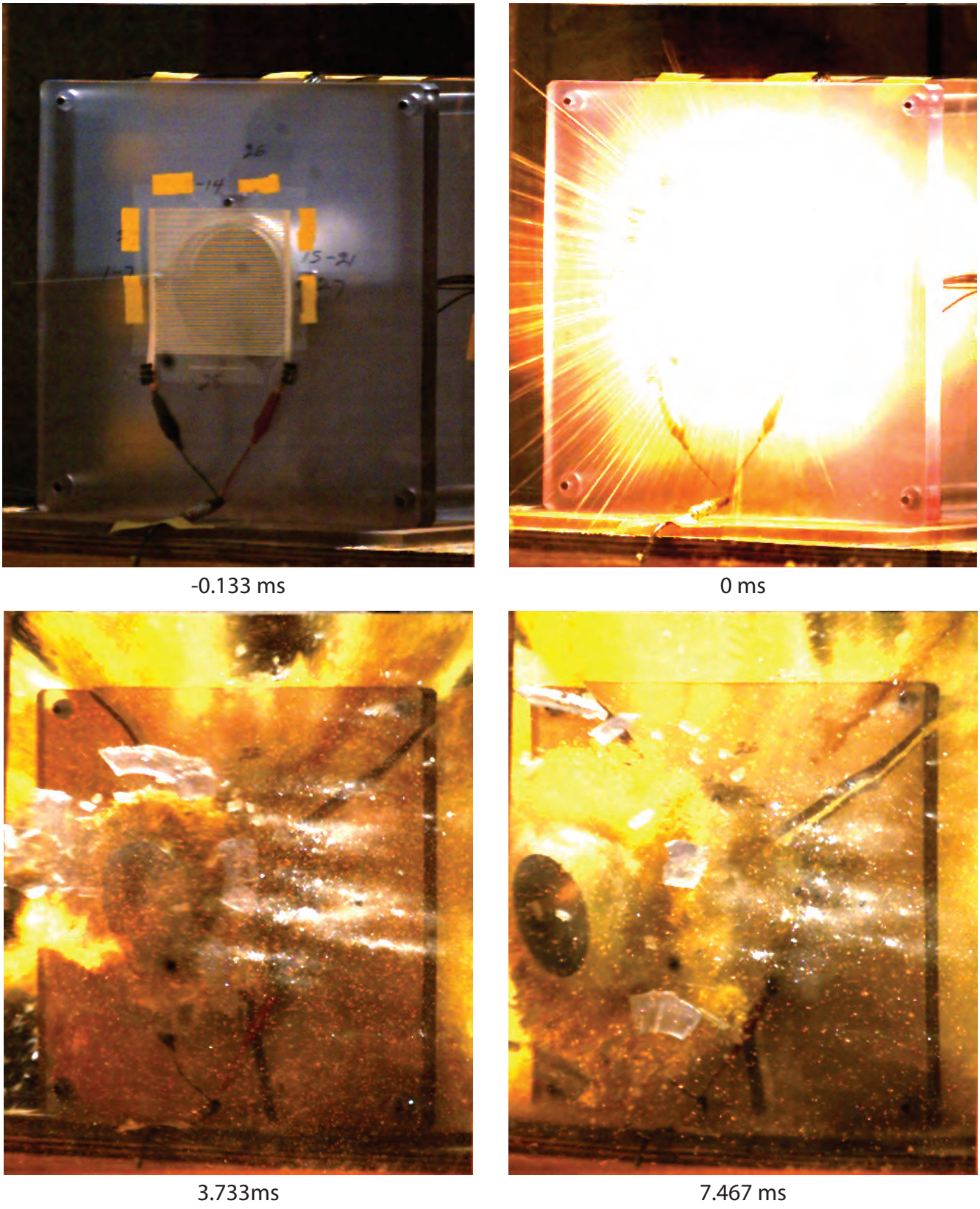

Figure 16: Frames from the high-speed video of K12-21570.

Figure 17: Post-shot photographs of the steel cylinder (left) and front plate (right). A small dent is visible on the face of the steel cylinder, though it is not deep.

were in contact with the steel cylinder. Only rail 1 returned signals on all pins, rail 2 only returned the first two pins, and rail 3 returned the first 3. It is unknown why pin 7 on rail 1 shows a much lower effective velocity than the other pins.

Figure 19 shows the measured velocities and positions of the back plate at the three probe locations. All the velocities are in the 30 to 50 m/s range, with displacements of 3 to 4 mm over the integration time.

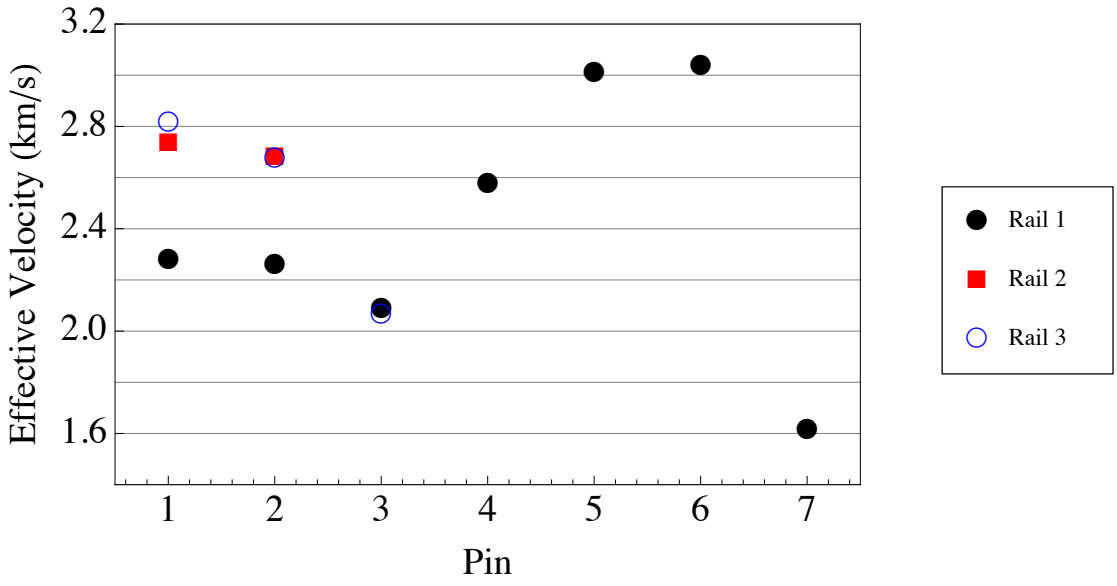

Figure 18: Effective velocity of the disturbance from the impact point, assumed to be in the center of the cylinder, to the pin location for shot K12-21570.

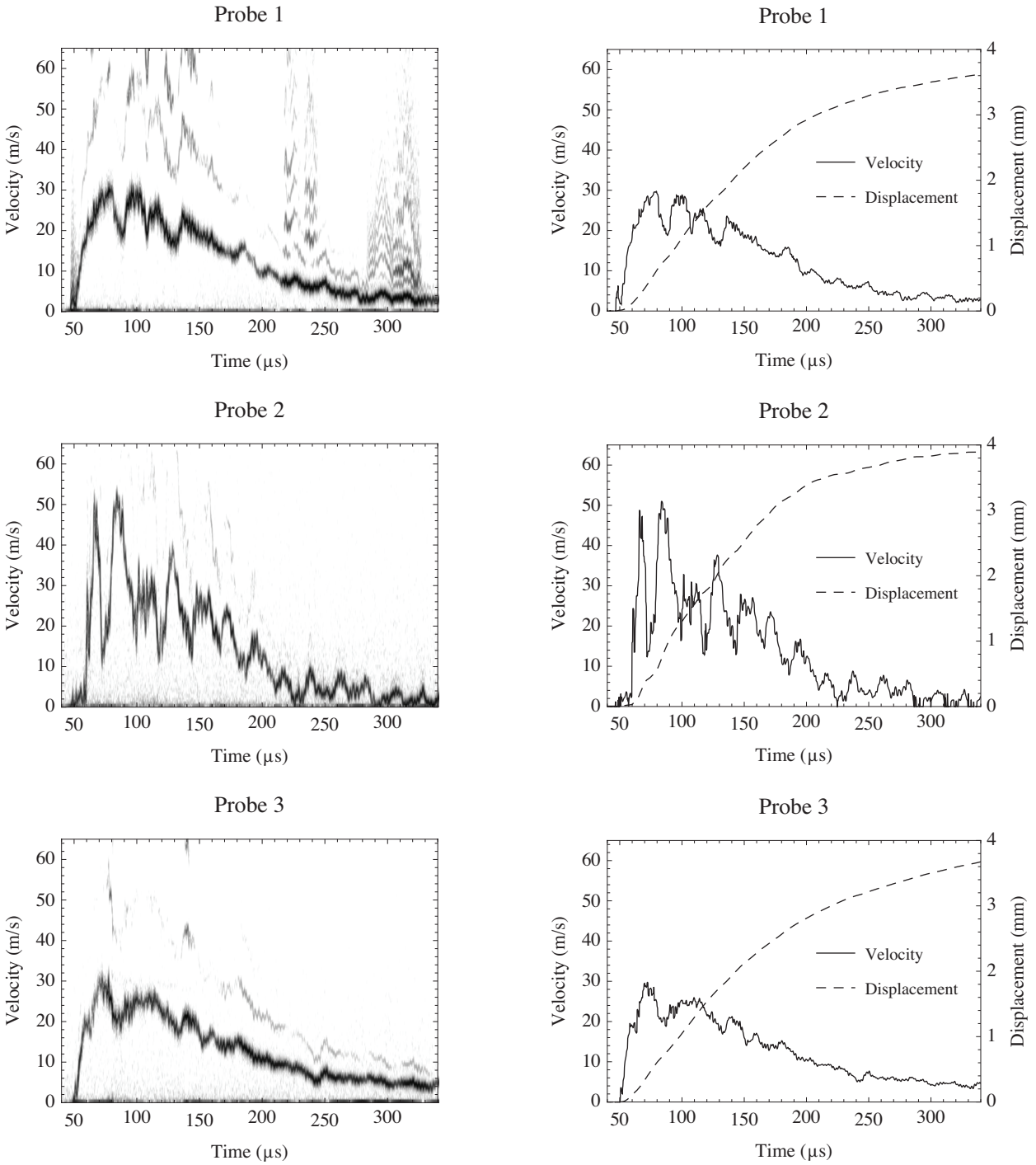

Figure 19: PDV data for K12-21570. The spectrograms are shown in the left column. Extracted velocities and integrated displacements are shown in the right column.

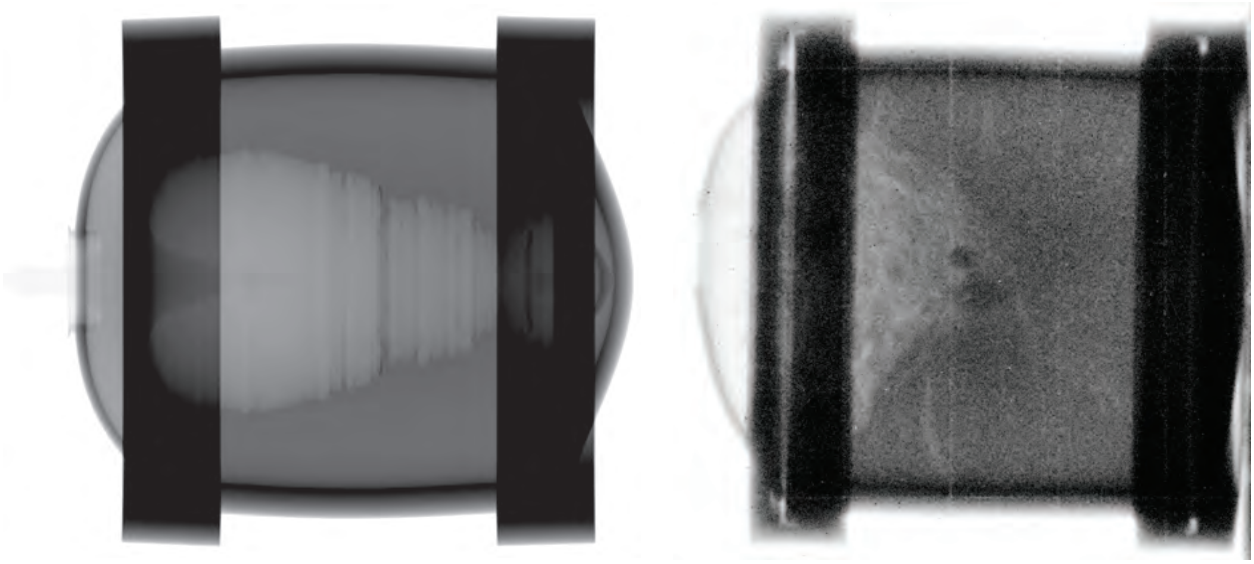

Figure 20: Comparison between CTH simulation and post-shot radiograph for shot K12-21556. The simulation image on the left shows the areal density of the object in the range from 0 to 50 g/cm^2.

4 CTH simulations

CTH simulations of both impacts were performed in 2D cylindrical coordinates using the History Variable Reactive Burn (HVRB) model for PBX-9502. In these simulations, detonation did not occur at impact velocities below approximately 3.7 km/s, which is beyond the capabilities of the 30-mm gun.

Figure 20 shows the areal density of a simulation of shot K12-21556 500 μs after a 2.5 km/s impact compared with a post-shot radiograph of the K12-21556 target from figure 13. In the simulation, the projectile has nearly reached the back plate of the target. Clearly, the simulation predicts that the projectile will penetrate much farther into the PBX-9502 than it actually does. The deformation of the front plate is similar in both simulation and experiment.

Figure 21 shows the areal density of a simulation of shot K12-21570 89 μs after projectile impact to match the time of the radiograph. The contrast range of the radiograph has been adjusted to better show the cavity inside the PBX-9502. Although this cavity is partially obscured by pin rails 1 and 3 as well as two of the four front-plate pins, the edge of the cavity is visible in the top half of the image. The cavity size is similar to that in the simulation. Qualitatively, the cavity shape is also similar, though the relative size of the cavity lobes is not correct. The simulation shows that the projectile does not penetrate into the steel cylinder behind the PBX-9502, which is also seen in the radiograph as well as the post-shot image of the steel cylinder (figure 17). The front plate is not visible in the radiograph since it is covered by the polycarbonate mounting plates.

5 Conclusions

Two experiments were performed impacting PBX-9502 in different configurations with a 1/2-inch diameter low-carbon steel sphere at velocities of 2.4 to 2.5 km/s. In both cases, the primary result is that the PBX-9502 did not detonate. High-speed video of the impacts shows that some PBX-9502 did react during the impact, though not enough to sustain a deflagration. PDV and

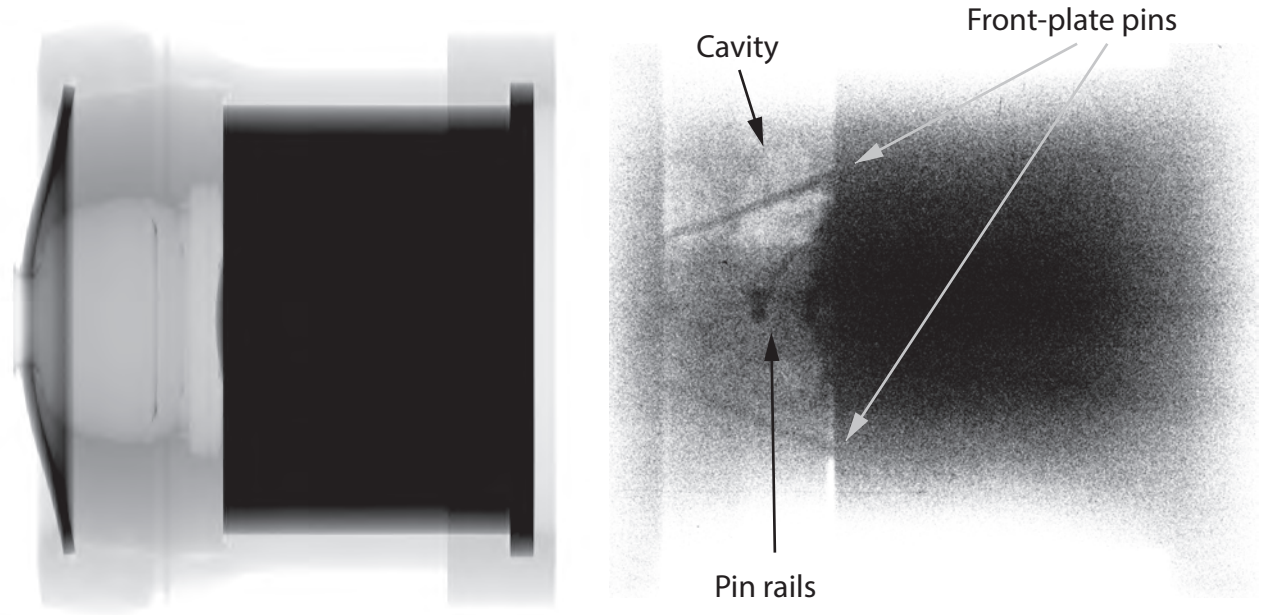

Figure 21: Comparison between CTH simulation (left) and dynamic radiograph (right) for shot K12-21570. The simulation image shows the areal density of the object in the range from 0 to 50 g/cm^2. Both images are at a time of 89 μs after projectile impact.

x-ray diagnostics were fielded primarily to be used in the event of an energetic reaction, but both diagnostics were entirely consistent with a non-energetic event. In the steel-cased configuration, post-shot measurement of the recovered mass gives an upper bound of 20 g for the amount of PBX-9502 that underwent a reaction. Post-shot collection of the PBX-9502 was not possible for the plastic-cased configuration.

The data from the piezoelectric pins are more ambiguous than the PDV or radiograph. Disturbances have multiple possible paths between the impact location and the pin location with no information as to which path was followed in the event. However, in shot K12-21556 effective velocities for pin rail 1 were consistenly higher than for the other two rails (figure 11). Post-shot radiographs of K12-21556 (figure 13) reveal the presence of cracks in the bulk of the PBX-9502. Perhaps the cracking allowed the disturbance to propagate to the pins in rail 1 faster than in the other rails. The pin data for K12-21570 is not as useful, as only the first two pins were in contact with the PBX-9502. All three rails show similar behavior for the first two pins. Only pin rail 1 returned data past the third pin, and it is unknown why pin 7 on rail 1 returned a much lower effective velocity than pin 6.

CTH simulations were also performed of the two configurations, and some aspects of these simulations agreed with the experimental data and some did not. The PBX-9502 did not detonate in either the simulation or the experiments, while the simulations did not agree with the experiments in the penetration depth.

References

[1] Jonathan L. Mace, "SMIS Logistics & SMIS 1.2 Summary. Yearly SMIS Cycles & Brief Data Summary," JMP MWFIR Review, SNL, Albuquerque, NM, LA-UR-07-6126, 2007

[2] Jonathan L. Mace, "SMIS Shot Series 3: N-9 3D threshold detonation experiments via 50 cal projectile insult," TCG-I, Eglin AFB, FL, LA-UR-09-2322, 2009

[3] Jonathan Lee Mace, "SMIS-3: N-9 Threshold Detonation Experiments via 50cal Projectile Insult," LANL, Los Alamos, NM, 2009